Article

Comprehensive Two-Dimensional Gas Chromatography with Mass Spectrometry: Towards a Super-Resolved Separation Technique

Yada Nolvachai, Laura McGregor, Natasha Damiana Spadafora, Nick Bukowski, and Philip John Marriott

Just Accepted

Comprehensive Two-Dimensional Gas Chromatography with Mass Spectrometry: Towards a Super-Resolved Separation Technique

Yada Nolvachai,[†] Laura McGregor,[‡] Natasha Damiana Spadafora,[§,ǁ] Nicholas P. Bukowski,[§] and Philip J. Marriott[†,*]

[†] Australian Centre for Research on Separation Science, School of Chemistry, Monash University, Wellington Road, Clayton, VIC 3800, Australia.

[‡] SepSolve Analytical, 4 Swan Court, Cygnet Park, Peterborough, PE7 8GX, United Kingdom

[§] Markes International, Gwaun Elai Medi-Science Campus, Llantrisant, RCT, CF72 8XL United Kingdom

[ǁ] Department of Ecology, University of Calabria, Laboratory of Plant Cyto-physiology, Ponte Pietro Bucci, I-87036 Arcavacata di Rende, Cosenza, Italy

Corresponding author email: philip.marriott@monash.edu

ABSTRACT: A data interpretation and processing approach for improved compound identification and data presentation in comprehensive two-dimensional gas chromatography (GC×GC) is described. A footprint peak of a compound in 2D space can be represented by a centroid or peak apex, similar to the data-reduced histogram spectra used in mass spectrometry. The workflow was demonstrated on data from GC×GC–TOFMS. Peaks in a modulated chromatogram were initially detected by conventional chromatographic integration, followed by a curve-fitting approach, which interpolated high-precision, absolute retention times for all modulated peaks. First dimension retention time (^1t_R) was obtained by using an exponentially-modified Gaussian (EMG) fitting model for near-Gaussian distributed sub-peaks, polynomial fitting for highly-asymmetrical peaks, and parabolic fitting for under-sampled peaks, which allows determination of a precise ^1t_R considering the dwell-time arising from modulation and ^2t_R. Area summation of the modulated peaks belonging to the same compound was then performed to yield the total peak area. Each compound in the GC×GC–MS result was then represented by its position at the intersecting coordinates, (^1t_R, ^2t_R), in the 2D separation plane, having a height of the same magnitude as the total component summed area. This results in a novel and uncluttered GC×GC output convention based on the scripted total ion chromatogram (TIC) data with precise ^1t_R, ^2t_R and area. Comparison between the contour plots from the scripted and conventional TIC revealed improved data presentation, accompanied by an apparent enhanced resolution. The described approach was applied to the identification of 177 aroma compounds from peaches as indicators of fruit quality.

Multidimensional gas chromatography (MDGC) and its comprehensive 2D variant (GC×GC) have made significant inroads into improved analysis of volatile compounds, based on the enhanced resolution that they offer.[1,2] The search for analytical methods that improve the separation of multi-component samples is the rationale for GC×GC, where improved separation corresponds to improved compound measurement. Comprehensive 2DGC is particularly 'disruptive' in that it offers very high total peak capacity,[3] alters the manner in which individual compounds are physically processed during the chromatographic separation by employing a modulation process, and requires a completely redesigned software interpretation of the result.[4]

Modulation is a unique aspect of GC×GC, and it is key to the experiment. There is now a reasonable choice of modulators available for GC×GC,[5] typically employing either thermal modulation, using a trapping process that is cooler than the prevailing GC oven temperature, or valve-based flow modulation which employs a sampling loop as a collection device. In all cases, the purpose of the modulator is to collect first column eluate (^{1}D) in a small time period, focus the analytes as a narrow band (in cryogenic systems), and then transfer the analytes on to the second column (^{2}D) containing a different stationary phase to the first column. This process usually (i) occurs at a period (the modulation period, P_M) faster than the peak width on the ^{1}D column, (ii) produces multiple modulated peaks for a single compound according to the modulation ratio (M_R), and (iii) elutes all the peaks from the ^{2}D column at a time < P_M.[6]

In general, GC×GC involves analysis of raw data of a modulated chromatogram arising from a sequential ^{1}D – ^{2}D separation. Components on the first column with a corresponding ^1t_R retention are modulated into a series of 'pulsed' peaks (sometimes referred to as 'sub-peaks' or 'peaklets') which are rapidly delivered to the ^{2}D column and subsequently recorded by a detector. As a result, a set of modulated peaks is obtained for each compound. Software is required to merge these sub-peaks and visualize the data as a contour (or colour) plot.

The modulation process produces a series of modulated peaks separated by the P_M value, for each ^{1}D component, however the manner in which the modulator samples across a ^{1}D peak depends on the timing of peak elution from the ^{1}D column. This is referred to as the phase of modulation,[7] and the pattern of

peaks generated may be defined as in-phase (a symmetrical sequence with a single maximum sub-peak), 180° out-of-phase (a symmetrical sequence of sub-peaks with two equal maxima), or any other intermediate phase. The Gaussian or exponentially-modified Gaussian model of the ^{1}D peak has been used to describe the modulation peak pattern, and allows prediction of ^1t_R, and other metrics of the compound.[8] Reproducibility of the analytical system allows relatively good correlation with slight variation in sampling phase of a ^{1}D peak.[9] Taking the maximum modulated peak as a surrogate for a ^{1}D compound retention will clearly be incorrect.

Peak capacity (n_c) in a GC×GC experiment must include the separation achieved on both ^{1}D and ^{2}D columns. The ^{1}D column normally has a high n_c value; the ^{2}D column may have a modest n_c due to its short length or very fast elution. Typical values might be 500 and 20 respectively. The multiplication of $^1n_c \times ^2n_c$ is believed to overestimate the total peak capacity since the effect of sampling across the ^{1}D peak must be included. 2D data presentation may be by 2D contour, 3D surface or apex plots.[10] The apex plot considers the peak maximum in 2D space, and this has been articulated in the literature. For example, use of a pixel-based approach for identification of the peak from a contour plot has been applied in GC Image software (Zoex).[11] Alternatively, straightforward approximation of ^1t_R and ^2t_R can be made from a linear chromatogram prior to the data transformation, as applied in software platforms such as ChromSpace (SepSolve Analytical) and ChromaTOF (LECO). This takes into account the modulator start time and all the successive release times so that a precise calculation of ^2t_R can be performed.

In this study, the latter approach is shown to provide accurate ^1t_R and ^2t_R values for the GC×GC–TOFMS analysis of volatiles from peaches. A novel data presentation approach was then proposed combining all the modulated peaks of the same compound into the centroid profile. Combining the use of centroid peak identification with filtering scripts enables data reduction of the total ion chromatogram (TIC), whereby a clean signal for a target compound is obtained with apparent improved resolution. The interpretation of the GC×GC result was compared with that obtained from the conventional TIC and extracted ion chromatogram (EIC) data. Comparison was then made in terms of noise level and apparent resolution of targeted compounds.

EXPERIMENTAL SECTION

Plant material, post-harvest storage conditions and sample preparation. Peach (*Prunus persica* L. Batsch *cv* Sagittaria) fruits were field-grown in Calabria (Italy). Fruits were harvested at the optimal commercial stage when the Brix value was above 8° and the firmness was below 6.5 kg cm^{-2} (63.7 N), as required by the European Union for the market of peaches (Commission Regulation EC, No.1861/2004 of 28 October 2004). After harvest, whole fruits were stored at 1 ℃ in the dark. Sampling was performed in triplicate after 14 days of storage at 1 ℃. Control samples were collected at harvest (day 0).

Collection and analysis of VOCs. Volatile organic compound (VOC) sampling was carried out as described previously.[12] At each time point eight peaches were placed in a multipurpose roasting bag (55 cm × 45 cm). Sampling on thermal desorption tubes (Tenax TA & Sulficarb, Markes

International Ltd., Llantrisant, UK) was carried out at the University of Calabria for three biological replicates at each time point from separate samples of peaches. Sorbent tubes were then capped and transported to Cardiff University for analysis. Tubes were desorbed on a TD-100 thermal desorption system (Markes International Ltd.) with the following conditions: 10 min at 280 °C, with a trap flow of 40 mL min^{-1} and for trap desorption and transfer to GC using 40 °C s^{-1} to 300 °C, with a split ratio of 6:1 into a GC (7890A, Agilent Technologies, Inc.).

GC×GC–TOFMS configuration. GC×GC analyses were carried out on a 7890A GC system coupled to a BenchTOF™ time-of-flight mass spectrometer (Markes International, Ltd.). The ion source temperature was set at 200 °C, the transfer line was set at 250 °C, with a mass range of m/z 35 to 350 and an acquisition rate of 50 Hz. The system was fitted with a reverse fill/flush INSIGHT® flow modulator (SepSolve Analytical, Peterborough, UK). The loop flush time was set to 100 ms with a modulation period of 2.5 s. The GC×GC column set consisted of: ^{1}D: MEGA-5 MS column (60 m × 0.32 mm I.D. × 0.5 μm film thickness (d_f)); ^{2}D: Stabilwax (3 m × 0.25 mm I.D. × 0.1 μm d_f). The GC oven ramp was set to: 40 °C (hold for 3 min), 4 °C min^{-1} to 250 °C (hold 15 min). A flow of 1.5 mL min^{-1} of helium inert carrier gas was applied to the ^{1}D column, with a post-primary split of 7.5:1, resulting in a flow into the modulator of 0.2 mL min^{-1} and a second column flow of 6 mL min^{-1} into the TOFMS. A retention time / index standard (C$_8$–C$_{20}$, Sigma Aldrich) was prepared by injection of 1 μL of the standard mixture directly onto a TD sorbent tube (Tenax TA, Sulficarb) and analysed under the same conditions as the samples. This intra-batch retention indexing (RI) standard was used to establish an initial RI calibration scheme. One of the peach data files was subjected to peak finding by global deconvolution, with tentative peak identifications, based on spectrum matching against the NIST 2017 database, were augmented by the software's parametric retention index penalty scheme. A severe RI penalty ('RI tolerance' of 15 and 'RI penalty rate' of *Very strong*), imparted orthogonal filtering to all spectrum matches, such that only those with intrinsically high spectrum match factors and closely-correlated experimental RIs with NIST reference values, would be accepted. Curated from this list of components, all intrinsic to peach volatiles, and with assured identities, a set of compounds with their associated retention indices can 'anchor' the 2D space and be captured for storage in the software, and called by all subsequent processing methods. This so-called 'RI pattern' allows for a rigorous splined RI calibration model, preserving great predictive accuracy at the transitions between the isothermal and ramped temperature phases of the GC oven program.

Software. Instrument control and data processing was performed using the ChromSpace® software platform (SepSolve Analytical, Peterborough, UK).

RESULTS AND DISCUSSION

Method design. Precision was of upmost importance in the experimental design to ensure confidence in the full process, from sample collection through to data interpretation. Triplicate analysis was performed for each peach variety to ensure sampling of a reproducible subset. For batched acquisition, the order of samples was randomised and interspersed with QC and procedural blanks. Since the total instrument time spanned

several days, retention indexing standards were added to the front and end of the batch.

For the choice of column set, a 60 m × 0.32 mm ID × 0.5 μm d_f of relatively high mass-loadability and highly-resolving ^{1}D column, operated under optimum linear velocity, was paired with a 3 m × 0.25 mm ID × 0.1 μm d_f low-impedance ^{2}D column, the latter enabling a relatively low output pressure to be maintained for the ^{1}D column. Vacuum termination of the ^{2}D column and the choice of phase ratio enabled a relatively high peak capacity to be maintained, delivering sharp 'sub-peaks' to the detector, in a sufficiently short modulation period to recover good resolution from the ^{1}D column. Most low-concentration solutes detected were modulated at least three times, *i.e.* a modulation ratio > 3.

The introduction of a post-^{1}D column split, just upstream of the modulator, enabled a one-dimensional high-resolution reference chromatogram to be recorded by FID monitor detector for all samples in the fruit quality project. The split flow ratio was maintained at 7.5:1, in favour of the 1D FID channel, such that the pneumatic compression ratio across the flow modulator was nominally 30:1, enabling rapid flushing of the filling loop into ^{2}D for good ^{2}D peak capacity.

In terms of the choice of modulator, flow modulation was preferred due to the absence of volatility discrimination – meaning that species from very volatile to low volatility are efficiently modulated.[13] Furthermore, flow modulation has been proven to deliver robust and repeatable analysis in projects spanning many days or weeks, as shown by the relative standard deviations in Table 1 (for ^1t_R, ^2t_R) for a selection of compounds in the peach volatilome.

Determination of ^2t_R and modulated peak area. The modulated chromatogram is divided into sequential modulation events, each of a given P_M as shown in Figure 1A. Both ^2t_R and the corresponding area are then calculated by peak integration for each modulated peak (Figure 1B).
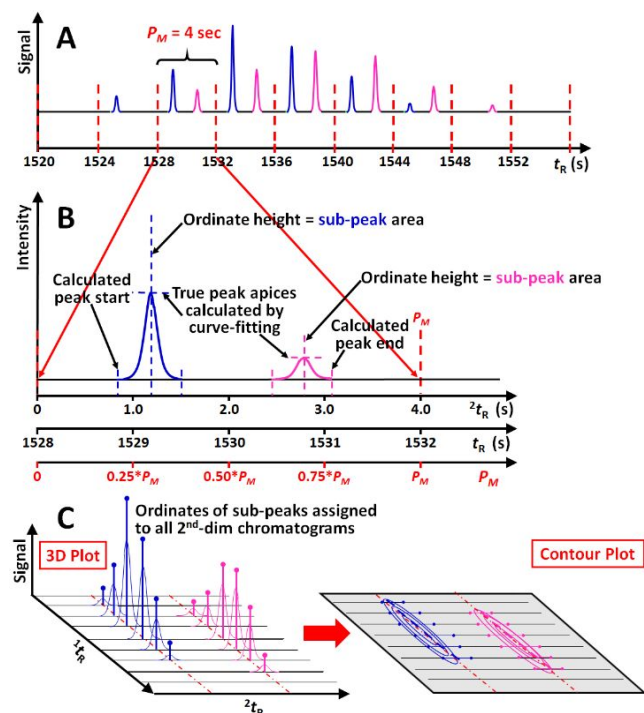

Figure 1. (A) An example modulated chromatogram comprising 9 modulation events of 4 s each. (B) Calculation of ^2t_R and area

determination of each modulated peak; a single modulation event is shown. (C) Corresponding plot of all modulated peak positions with their calculated centroids in a plot transformed into 3D, and an analogous surface contour plot.

The t_R of a modulated peak (referred to as a sub-peak here) may be approximated by means of parabolic curve fitting and was applied for a near-Gaussian peak shape, with polynomial fitting applied for asymmetrical peaks. By taking into account the modulator starting time for the nth modulation, precise calculation of ^2t_R (or position ordinates on the ^2t_R axis, *x*-axis) of each sub-peak ($^2t_{R,n}$) with *n* modulations, since each modulation will have very slight differences in ^2t_R due to incremented oven temperature, can be obtained using eq1. Not to be confused with modulation, mod here is a mathematical operator, modulo.

$$(t_R \text{ of modulated peak}) \bmod (n \times P_M) = {^2t_{R,n}} \qquad (1)$$

The area (*s*, ordinate intensity) of each modulated peak (*y*-value, height) is obtained as the integrated area of a modulated peak. The ^2t_R and area data of all the modulated peaks can be combined and transformed into 3D as shown in Figure 1C. Centroids, as defined in this paper, essentially capture apex positions and abundances of their precursor integrals. The complementing metadata recorded from classical integration (including deconvolution) includes footprints (for GC×GC data) and basal peak widths, for all modulated peaks (sub-peaks), all of which are preserved/embedded in the qualitative/quantitative workflows and accessible for reporting/export/laboratory information management system (LIMS) upload of sample results.

It should be noted that due to the short modulation period, ^{2}D separation can be assumed to be isothermal.[14] Successive modulation events for a given component occur at incremented oven temperature and so the ^2t_R value will be slightly less for successive modulations; ^2t_R of the compound is initially approximated by a weighted average of the ^2t_R values of all the modulated peaks corresponding to the same compound according to eq 2:

$$^2t_R = \frac{(s_1 \times {^2t_{R,1}}) + (s_2 \times {^2t_{R,2}}) + (s_3 \times {^2t_{R,3}}) + \dots + (s_n \times {^2t_{R,n}})}{s_1 + s_2 + s_3 + \dots + s_n} \qquad (2)$$

However, in order to assign reliable and reproducible ^2t_R values to reported solutes that may range widely in concentration and suffer column loadability-induced (overloading) distortion, only a subset of modulated solute peaks, centred on the sub-peak of maximum ordinate intensity, are used for the final ^2t_R peak assignment.

Determination of ^1t_R and compound total peak area. From the modulated chromatogram of peach volatiles, all the detected peaks were integrated and their ordinate intensities were plotted against the ^1t_R axis. Note that all the sub-peaks of different compounds in the same modulation event with any given ^2t_R were assigned to have identical ^1t_R values here, since they arise at the same sampled zone on the ^{1}D column. Peak shapes of the ^{1}D separation were approximated by using curve fitting. To this end, EMG (or parabolic) fitting was applied for near-Gaussian sub-peaks; whilst, polynomial approximation was applied for highly asymmetrical peaks. An example is shown in Figure 2.
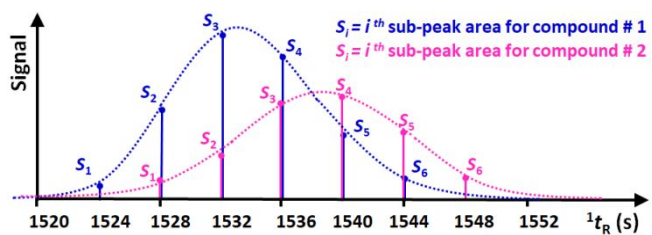
Figure 2. Approximation of peak shape in ^{1}D separation from the ordinate intensities of modulated peaks (sub-peaks) by using EMG curve fitting.
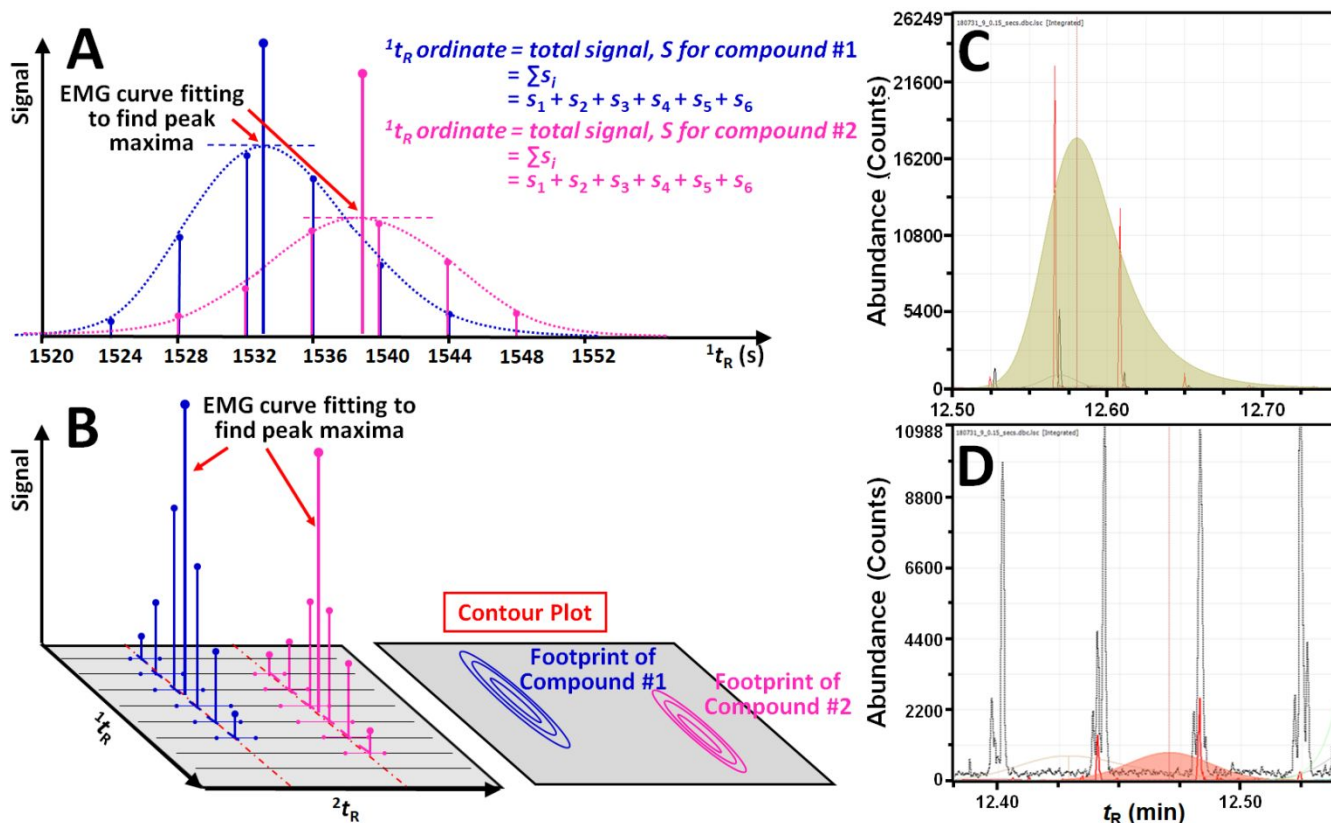
Figure 3. (A) Approximation of ^1t_R and total intensity of compounds from the modulated chromatogram, with (B) the corresponding plot of the compound positions (centroids) in a contour plot shown as the highest ordinates. (C) Example of EMG construction and fitting to a modulated compound exhibiting tailing on the primary column, and (D) example of EMG construction and fitting to a modulated compound of low signal abundance.

According to the curve fitting process, the compound ^1t_R (position on the x-axis) can be predicted as the apex position of the fitted peak, and the total intensity (^1t_R ordinate) can then be calculated by summation of all the modulated peak intensities belonging to the same compound as shown in Figure 3A. The estimation of compound ^1t_R values with their corresponding total intensities can be transformed and replotted on a contour plot shown in Figure 3B. Further information containing examples of the EMG construction and fitting to modulated compound integrals, from other modulator types, such as thermal modulators is shown in Figure S1–S3, Supporting Information.
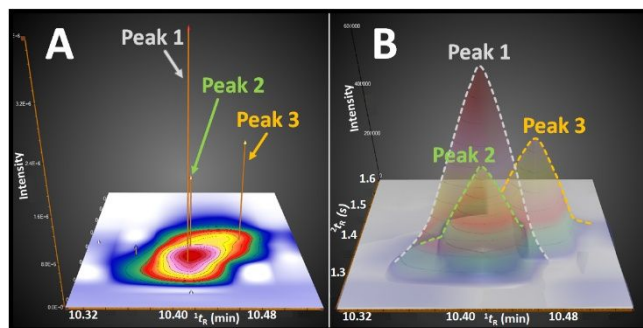

Figure 4. (A) Overlay of determined compound positions (given as centroids) within an enhanced TIC region of the contour (colour) plot for volatiles from peaches. (B) Deconvolved 3D peak integrals, charted as semi-opaque response surfaces of the 3 coeluting compoents marked in (A), here generating 3 overlapping response surfaces.

This approach was applied for generation of the centroid-based result[15] for the volatiles from peaches as shown in Figure 4. Ordinate positions on the source chromatogram correspond to their precisely interpolated ^1t_R and ^2t_R coordinates for a given chromatographic analysis. In addition, each centroid also contains the overall MS spectrum of each compound facilitating simple compound identification.

Generation of filtered GC×GC result from scripted TIC and comparison with conventional TIC and EIC. Conventionally, a single or even multiple mass constraint can be applied to TIC of the GC×GC result, such that this will result in an extracted ion chromatogram (EIC) of the result which can be transformed to specifically indicate compound positions with different target mass(es) in a contour plot. Thus, chemical classes or compounds that possess a given fragment mass can be uniquely displayed. More effective peak filtering methods can be performed based on extraction of several m/z values with a fixed ratio of their intensities.

γ-Dodecalactone in a peach sample with the 2D TIC plotshown in Figure 5A may be taken as an example. The conventional EIC analysis using m/z 85 (which is the base m/z peak common to γ-lactone) is shown in Figure 5B. By applying the filtering criterion shown in Figure S3, Supporting Information, Figure 5C shows a clearer 3D contour signal for target compounds than a conventional EIC approach (Figure 5B). Combined with the peak filtering approach, the centroid data with the underlying 2D contour can be generated with more confidence as shown in Figure 5D.
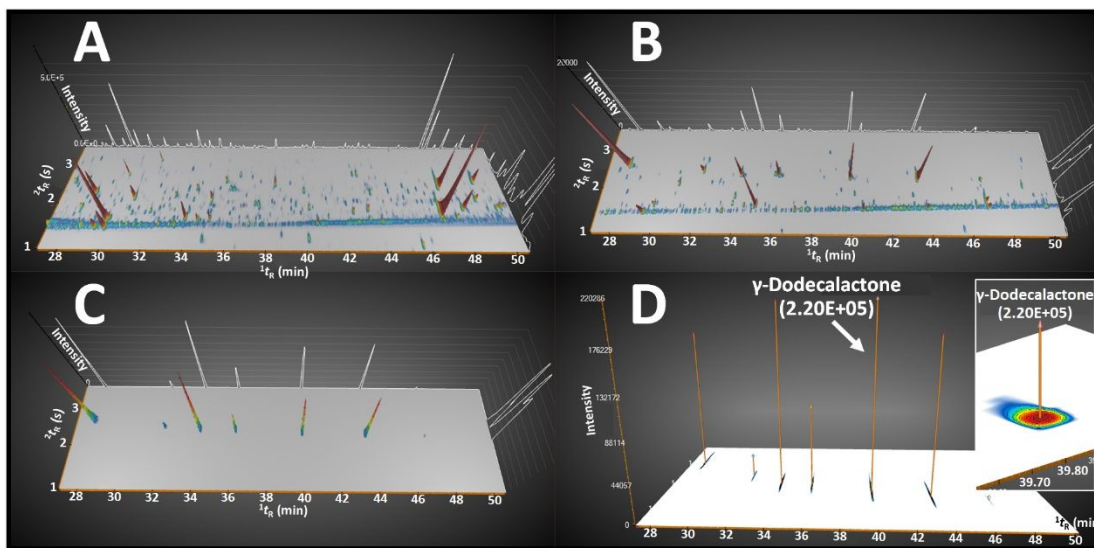
Figure 5. GC×GC results of peach sample: (A) TIC, (B) EIC of the ion *m/z* 85 (profile data), (C) filtered TIC (profile data) with criterion shown in Figure S3, Supporting Information, and (D) filtered TIC showing integrated lactone peaks as centroids and 2D contour image.
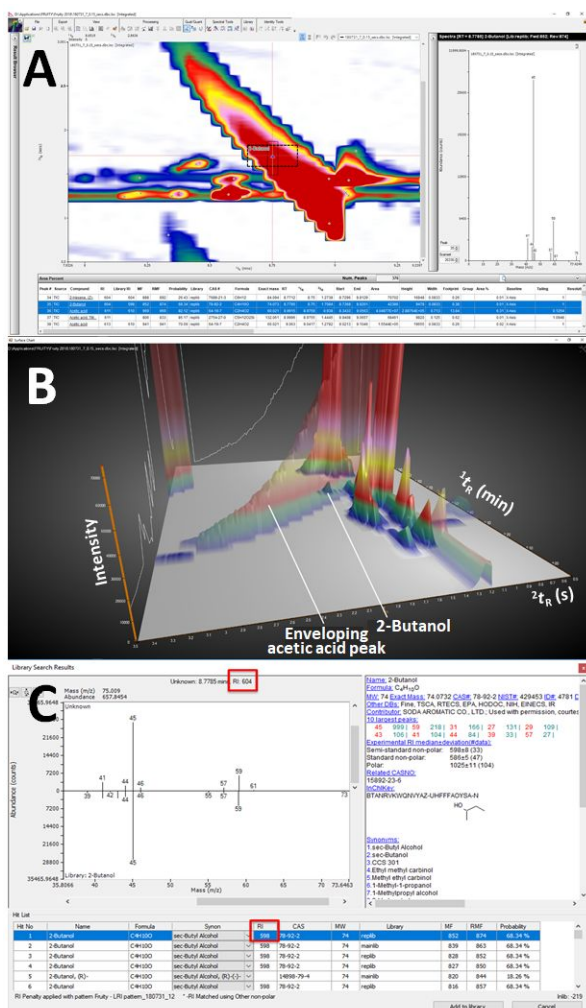

Figure 6. An example of the use of the centroiding approach to uncover a minor masked component in peach aroma. (A) Screen capture colour plot showing the overloaded acetic acid component (a GC trace and data report is also captured). (B) 3D surface plot highlighting the masked 2-butanol arrowed. (C) Mass spectrum library-matching against NIST17 (with various report data), constrained using the retention index scheme.

Practical sample analysis: compound identification (use of MS library match and ^{1}D retention index). A compound can be tentatively identified for each peak in a GC analysis providing that the peak's mass spectrum can be suitably matched with that from the NIST library. This is a necessary, but insufficient condition for identification. In addition, ^{1}D retention can be used to improve reliability of compound location in the 2D plot, and retention indices in both dimensions adds further certainty.[16] In this study, alkane standards were also analysed and their signal on the contour plot can be extracted by using multiple parametric filters (Figure 5). This allows improved estimation of ^1I values, to further support peak identification. The ^1I 'alkane grid' becomes a calibrating overlay for the peach VOC profile. By application of the peak filtering approach, 177 verified aroma compounds can be tentatively identified.

Figure 6 demonstrates the value of this approach, whereby a minor component (2-butanol) is enveloped within the overloaded acetic acid, but is still reliably centroided and identified using the retention index scheme. Figure 6A is a screen capture of the default data browsing user interface (UI), comprising 2D chromatogram, as a contour (colour) plot, with dynamic-links to spectral and tabular view-ports. In the chromatogram viewer, an expanded local region of TIC is centred on the dominating diagonal feature, an acetic acid peak, highly-distorted due to its overloading of the primary column. The cross-hairs mark the position of a found minor constituent, 2-butanol, with its corresponding mass spectrum charted. The table view-port shows these two constituents, acetic acid and 2-butanol, highlighted, revealing a 3-orders difference in their relative abundances. Figure 6B shows a linking view-port of the chromatographic range, as a 3D surface chart, with the opacity setting for the acetic acid integrated peak reduced to reveal the 2-butanol beneath. Figure 6C is the on-demand extended library browser, that can be launched from any of the linking view-ports, and showing the library hit ranking for 2-butanol, constrained by a difference penalty of its experimentally-determined linear retention index ($^1RI_{exp} = 604$) compared with its reference index, accessed from the NIST17 mass spectrum library ($^1RI_{ref} = 598$).

Table 1. Reproducibility of ^1t_R and ^2t_R of some identified aroma compounds in peach ($n = 8$), based on the centroid approach, and their respective relative standard deviation percentage (%RSD). Note that the samples used to generate these reproducibility metrics were taken from randomised peach samples representing a range of post-harvest storage durations. The range of individual compound concentrations across the 8 replicates was significant, and up to multiple orders of magnitude difference in some cases. The high mass loadability of the chosen column-set, and a dedicated independent pneumatic control for each column, resulted in the high degree of precision observed.

Compound	^1t_R (min)								
	Rep 1	Rep 2	Rep 3	Rep 4	Rep 5	Rep 6	Rep 7	Rep 8	%RSD
1,3-Pentadiene	7.073	7.073	7.073	7.083	7.083	7.074	7.075	7.074	0.064
2,3-Butanedione	8.441	8.433	8.436	8.441	8.436	8.440	8.436	8.437	0.035
n-Hexane	8.570	8.569	8.569	8.570	8.572	8.571	8.568	8.571	0.014
Ethyl acetate	9.053	9.053	9.053	9.053	9.054	9.055	9.053	9.055	0.010
1-Penten-3-ol	11.426	11.425	11.426	11.426	11.423	11.424	11.425	11.427	0.010
3-Methylbutanol	13.508	13.510	13.509	13.509	13.508	13.510	13.510	13.511	0.007
1-Pentanol	14.863	14.863	14.865	14.875	14.875	14.875	14.863	14.875	0.041
Isobutyl acetate	15.108	15.105	15.110	15.110	15.109	15.111	15.105	15.111	0.016
Butyl acetate	16.926	16.908	16.927	16.927	16.927	16.927	16.925	16.927	0.039
1-Hexanol	19.468	19.468	19.469	19.469	19.469	19.469	19.468	19.470	0.003
3-Methylbutyl ester	19.782	19.781	19.782	19.783	19.782	19.783	19.781	19.800	0.033
Pentyl acetate	21.427	21.430	21.427	21.432	21.432	21.430	21.430	21.434	0.011
n-Decane	25.261	25.260	25.261	25.261	25.261	25.260	25.260	25.259	0.003
Hexyl acetate	25.879	25.899	25.896	25.857	25.860	25.894	25.895	25.896	0.066
2-Ethylhexanol	26.605	26.613	26.611	26.603	26.603	26.608	26.606	26.614	0.016
n-Tetradecane	40.572	40.570	40.571	40.571	40.571	40.573	40.570	40.572	0.003

Compound	^2t_R (s)								
	Rep 1	Rep 2	Rep 3	Rep 4	Rep 5	Rep 6	Rep 7	Rep 8	%RSD
1,3-Pentadiene	1.284	1.275	1.268	1.279	1.274	1.268	1.283	1.266	0.551
2,3-Butanedione	1.614	1.607	1.597	1.606	1.596	1.598	1.612	1.597	0.446
n-Hexane	1.267	1.262	1.250	1.260	1.252	1.253	1.267	1.251	0.548
Ethyl acetate	1.431	1.424	1.414	1.422	1.417	1.417	1.430	1.415	0.474
1-Penten-3-ol	2.040	2.033	2.023	2.029	2.022	2.025	2.037	2.021	0.354
3-Methylbutanol	2.027	2.019	2.009	2.016	2.011	2.011	2.025	2.009	0.352
1-Pentanol	2.070	2.061	2.052	2.059	2.055	2.056	2.066	2.052	0.326
Isobutyl acetate	1.474	1.467	1.458	1.467	1.461	1.463	1.474	1.460	0.426
Butyl acetate	1.515	1.505	1.498	1.506	1.501	1.502	1.515	1.500	0.434
1-Hexanol	2.008	2.000	1.990	1.997	1.993	1.994	2.007	1.991	0.335
3-Methylbutyl ester	1.516	1.509	1.499	1.506	1.502	1.503	1.516	1.507	0.405
Pentyl acetate	1.542	1.536	1.525	1.533	1.528	1.529	1.544	1.528	0.441
n-Decane	1.415	1.410	1.399	1.406	1.401	1.403	1.417	1.400	0.492
Hexyl acetate	1.571	1.563	1.554	1.552	1.552	1.559	1.571	1.556	0.501
2-Ethylhexanol	1.860	1.851	1.843	1.851	1.847	1.846	1.856	1.847	0.305
n-Tetradecane	1.557	1.551	1.544	1.549	1.545	1.546	1.558	1.544	0.359

Reproducibility. The average of ^1t_R and ^2t_R of multiple replicates ($n = 8$) (Table 1) were used for the estimation of error from the centroid approach. The technique is shown to have excellent reproducibility with %RSD in the range of 0.003–0.066% and 0.305–0.551% for ^1t_R and ^2t_R respectively. For instance, the precision of the ^{1}D retention is not defined by the modulation period zone in which an analyte is located, but is given a precise elution time on the column. Thus, for butyl acetate data, the retention time range is 0.019 min (~1.1 s) and standard deviation of 2.3 s. Accurate retention attribution to compounds in the GC analysis effectively means that no chromatographic information (*i.e.* retention) is lost on the ^{1}D column, and by extension it follows that peak capacity is likewise not affected. This is in contrast to the belief that peak

capacity is affected by the sampling process in comprehensive chromatography analysis; our approach maintains chromatographic integrity of the ^{1}D column data. As expected, higher %RSD of ^2t_R was observed due to a smaller timescale in ^{2}D. In general, there is no significant relationship between %RSD error and other parameters such as elution time and compound class. The significance of this is that it essentially provides to the first dimension peak a retention precision that reflects a classical 1D peak retention time (Table 1). Thus, the modulation process need not impose a reduced peak capacity on the first column, since peak precision is maintained. This depends of course on accurate curve fitting of the modulated peak, and for overlapping ^{1}D compounds, on their degree of ^{2}D separation (or selecting unique m/z ions with MS). With accurate centroiding, it is possible that this indeed increases the peak capacity of the ^{1}D column by precise location of many more peaks; this will be considered elsewhere. It is well recognized that each individual modulated peak has a very precisely reproduced retention time, since this is determined by the timing of introduction into the ^{2}D column, and the short length of this column.[8,17] However, ^1t_R prediction depends on the phase of modulation, and the area values of the modulated peaks, and as shown in Table 1, this can be predicted with excellent certainty.

CONCLUSIONS

A new data analysis approach in GC×GC has been demonstrated, with filtering and automated generation of peak centroid points, and should result in improved peak identification. Importantly, the peak centroid location for both the ^{1}D and ^{2}D column predicts a very precise location of a component in the 2D space. With the developed script here, the approach was successfully applied for identification of 177 aroma compounds from peaches. The described workflow provides more precise determination of peak positions in GC×GC, while the centroiding approach can be considered as a higher separation – a super-resolved – concept for the separation space, with each compound represented as a discrete point in the 2D space in comprehensive 2D gas chromatography.

ASSOCIATED CONTENT

Supporting Information

The Supporting Information is available free of charge on the ACS Publications website.

Examples of the EMG construction and fitting to modulated compound integrals (PDF)

AUTHOR INFORMATION

Corresponding Author

* Email: philip.marriott@monash.edu
Notes
Authors LM, and NB and NDS are employees of SepSolve Analytical and Markes International, respectively. The software used to interpret chromatographic data, such as peak centroiding calculations and determination of accurate ^1t_R times have been incorporated into the ChromSpace package of Markes / SepSolve. The concepts of using modulated peak distributions to calculate accurate ^1t_R times derived from original research of the corresponding author.

REFERENCES

(1) Marriott, P. J.; Chin, S. T.; Maikhunthod, B.; Schmarr, H. G.; Bieri, S. Multidimensional gas chromatography. *TrAC, Trends Anal. Chem.* **2012**, *34*, 1-20.

(2) Adahchour, M.; Beens, J.; Vreuls, R. J. J.; Brinkman, U. A. T. Recent developments in comprehensive two-dimensional gas chromatography (GC×GC): IV. Further applications, conclusions and perspectives. *TrAC, Trends Anal. Chem.* **2006**, *25*, 821-840.

(3) Adahchour, M.; Beens, J.; Vreuls, R. J. J.; Brinkman, U. A. T. Recent developments in comprehensive two-dimensional gas chromatography (GC × GC). I. Introduction and instrumental set-up. *TrAC, Trends Anal. Chem.* **2006**, *25*, 438-454.

(4) Amaral, M. S. S.; Nolvachai, Y.; Marriott, P. J. Comprehensive Two-Dimensional Gas Chromatography Advances in Technology and Applications: Biennial Update. *Anal. Chem.* **2020**, DOI: 10.1021/acs.analchem.9b05412.

(5) Sharif, K. M.; Chin, S. T.; Kulsing, C.; Marriott, P. J. The microfluidic Deans switch: 50 years of progress, innovation and application. *TrAC, Trends Anal. Chem.* **2016**, *82*, 35-54.

(6) Nolvachai, Y.; Kulsing, C.; Sharif, K. M.; Wong, Y. F.; Chin, S.-T.; Mitrevski, B.; Marriott, P. J. Multi-column trajectory to advanced methods in comprehensive two-dimensional gas chromatography. *TrAC, Trends Anal. Chem.* **2018**, *106*, 11-20.

(7) Ong, R. C. Y.; Marriott, P. J. A review of basic concepts in comprehensive two-dimensional gas chromatography. *J. Chromatogr. Sci.* **2002**, *40*, 276-291.

(8) Adcock, J. L.; Adams, M.; Mitrevski, B. S.; Marriott, P. J. Peak modeling approach to accurate assignment of first-dimension retention times in comprehensive two-dimensional chromatography. *Anal. Chem.* **2009**, *81*, 6797-6804.

(9) Shellie, R. A.; Xie, L. L.; Marriott, P. J. Retention time reproducibility in comprehensive two-dimensional gas chromatography using cryogenic modulation - An intralaboratory study. *J. Chromatogr. A* **2002**, *968*, 161-170.

(10) Marriott, P. J.; Schoenmakers, P.; Wu, Z. Y. Nomenclature and conventions in comprehensive multidimensional chromatography- an update. *LC-GC Eur.* **2012**, *25*.

(11) GC Image LLC, GCxGC Blob Metadata and Statistics in GC Image. https://www.gcimage.com/gcxgc/usersguide/statistics.pdf (accessed 28/01/2020).

(12) Amaro, A. L.; Spadafora, N. D.; Pereira, M. J.; Dhorajiwala, R.; Herbert, R. J.; Müller, C. T.; Rogers, H. J.; Pintado, M. Multitrait analysis of fresh-cut cantaloupe melon enables discrimination between storage times and temperatures and identifies potential markers for quality assessments. *Food Chem.* **2018**, *241*, 222-231.

(13) Griffith, J. F.; Winniford, W. L.; Sun, K.; Edam, R.; Luong, J. C. A reversed-flow differential flow modulator for comprehensive two-dimensional gas chromatography. *J. Chromatogr. A* **2012**, *1226*, 116-123.

(14) Nolvachai, Y.; Kulsing, C.; Marriott, P. J. In Silico Modeling of Hundred Thousand Experiments for Effective Selection of Ionic Liquid Phase Combinations in Comprehensive Two-Dimensional Gas Chromatography. *Anal. Chem.* **2016**, *88*, 2125-2131.

(15) Blumberg, L. M. Metrics of separation performance in chromatography. Part 1. Definitions and application to static analyses. *J. Chromatogr. A* **2011**, *1218*, 5375-5385.

(16) Bieri, S.; Marriott, P. J. Generating multiple independent retention index data in dual-secondary column comprehensive two-dimensional gas chromatography. *Anal. Chem.* **2006**, *78*, 8089-8097.

(17) Xie, L.; Marriott, P. J.; Adams, M. Chemometric analysis of comprehensive two-dimensional gas chromatography data using cryogenic modulation. *Anal. Chim. Acta* **2003**, *500*, 211-222.

TOC Image